Uncertainties of soil moisture in historical simulations and future projections

Shanjun Cheng[1], Jianping Huang[1*], Fei Ji[1], Lei Lin[2]

1. Key Laboratory for Semi-Arid Climate Change of the Ministry of Education,

College of Atmosphere Sciences, Lanzhou University, Lanzhou, China

2. Department of Atmospheric Sciences, Sun Yat-sen University, Guangzhou, China

[*] Corresponding author address: Jianping Huang, College of Atmosphere Sciences, Lanzhou University, Lanzhou, 730000, China
E-mail: hjp@lzu.edu.cn

Abstract

Uncertainties of soil moisture in historical simulations (1920 – 2005) and future projections (2006 – 2080) were investigated using the outputs from the CMIP5 (Coupled Model Intercomparison Project Phase 5) and CESM (Community Earth System Model). The results showed that soil moisture climatology varies greatly among models despite the good agreement between the ensemble mean of simulated soil moisture and the GLDAS (Global Land Data Assimilation System) data. The uncertainties of initial conditions and model structure showed similar spatial patterns and magnitudes, with high uncertainties in dry regions and low uncertainties in wet regions. In addition, the long-term variability of model structure uncertainty rapidly decreased before 1980 and increased thereafter, but the uncertainty in initial conditions showed an upward trend over the entire time span. The model structure and initial conditions can cause uncertainties at all time scales. Despite these large uncertainties, almost all of the simulations showed significant decreasing linear trends in soil moisture for the 21st century, especially in the Mediterranean region, northeast and southwest South America, southern Africa, and southwestern USA.

1. Introduction

Soil moisture is widely recognized as a key parameter in environmental processes because of its important role in controlling the water and energy balance between the land surface and atmosphere [*Seneviratne et al.*, 2010]. Soil moisture generally refers to the amount of water stored in unsaturated soil zone, although it has different definitions in diverse fields, e.g., hydrology, meteorology, ecology. Soil moisture has a significant impact on evapotranspiration rate, soil thermal parameters, surface albedo, and Bowen ratio, and therefore affects the planetary boundary layer regime, clouds, and precipitation [*Cook et al.*, 2006; *Findell and Eltahir*, 2003a; b; *Guan et al.*, 2009]. Meanwhile, as the immediate water source for vegetation, soil moisture impacts the productivity and survival of plants [*Ciais et al.*, 2005; *Reichstein et al.*, 2007]. Therefore, it is important to study soil moisture and its variability to understand climate change and land–atmosphere interactions.

Traditionally, changes in soil moisture and its relationship with the climate system were studied via ground-based measurements [*Huang et al.*, 2008; *Wang et al.*, 2010]. Accurate soil moisture observation is essential for hydrological monitoring and forecasting, water resource management, and improvement of land surface models. However, in situ soil moisture measurements are unavailable for many large regions of the world, which limits the use of soil moisture observations. Remote sensing of soil moisture from satellites is becoming more prevalent to compensate for the lack of in situ observations [*Dorigo et al.*, 2012; *Wagner et al.*, 2003], but a great deal of work is still needed to address the uncertainty caused by inversion algorithms used in processing satellite signals. In addition, satellite-based soil moisture data are limited to the top soil, which is unsatisfactory for many climate applications.

Therefore, analyses of soil moisture changes and related hydrological variations in large spatial domains, and on interannual to decadal time scales, are mainly dependent on the outputs of model simulations [*Sheffield and Wood*, 2008; *Yang et al.*, 2007; *Yang et al.*, 2011], because modeled soil moisture can yield gridded values and includes deep soil layers.

However, the quality of model output is affected by uncertainties in meteorological forcing and parameter inputs, as well as by inadequacies in model physics [*Li et al.*, 2012]. In particular, soil moisture is a complex variable, with a dynamic range defined by specific precipitation, evaporation, and runoff formulations utilized in a given model [*Koster and Milly*, 1997]. Marked differences are seen in the soil moisture products generated by different models, even when the models are driven by precisely the same meteorological forcing [*Dirmeyer et al.*, 2006]. Given these differences, it is necessary to validate simulated soil moisture against observed datasets, and compare soil moisture from different models. Understanding uncertainties in climate models during analysis of climate change and its impacts is a topic of fundamental importance, and has therefore attracted a great deal of attention.

Model uncertainties arise from inaccuracies in model structure, initial conditions (or ensemble runs), and greenhouse gas emission scenarios used [*Woldemeskel et al.*, 2012]. To evaluate the uncertainty of a model's structure, outputs of dozens of Earth System Models (ESMs) from the Coupled Model Intercomparison Project Phase 5 (CMIP5), coordinated by the World Climate Research Programme (WCRP) in support of the Intergovernmental Panel on Climate Change's Fifth Assessment Report (IPCC AR5), were used in this study. CMIP5 promotes a set of model simulations to understand the differences and uncertainties in model

simulations and projections [*Taylor et al.*, 2012]. Over the past few years, there has been a great deal of progress in the performance of CMIP5 simulations and projections [*Ahlström et al.*, 2012; *Bracegirdle et al.*, 2014; *Orlowsky and Seneviratne*, 2013], mainly focusing on temperature and precipitation [*Aloysius et al.*, 2016; *Knutti and Sedláček*, 2013; *Kusunoki and Arakawa*, 2015; *Woldemeskel et al.*, 2016]. In addition, almost all research regarding the uncertainties of temperature and precipitation is focused on future projections, because observations for temperature and precipitation are sufficient. The accuracy of historical temperature and precipitation simulations can be verified by sufficient observation data. However, for soil moisture, a key and more complex variable in environmental processes, its in situ observations are lacking, and there have been relatively few studies. It is necessary to study uncertainties in simulated soil moisture, not only in future projections, but also in historical simulations. However, most ESMs of CMIP5 have only a few (or even one) ensemble runs, which is not sufficient to study the uncertainty of initial conditions. To compensate for this shortage, 30 ensemble members of perturbation simulations using the Community Earth System Model (CESM) [*Hurrell et al.*, 2013] were used in this study. Note that these are CESM runs we carried out, not the ones officially archived by the CMIP5.

In this study, we examined the performance of the CMIP5 and CESM in simulating soil moisture, and investigated the uncertainties in model structure and initial conditions. We examined the accuracy of soil moisture simulated by multiple models for historical simulations (1920 – 2005) against the Global Land Data Assimilation System (GLDAS) data, focusing on climatological means and trends in soil moisture. We also studied the uncertainties among multiple models for historical simulations and future projections over the

21st century (2006 – 2080) forced by the Representative Concentration Pathways 4.5 (RCP4.5) and 8.5 (RCP8.5) simulation scenarios. The paper is organized as follows. The analyzed datasets and methods are described in Section 2. The results are shown in Section 3. A summary and discussion are provided in Section 4.

2. Dataset and methods

2.1 CMIP5 outputs

The simulated monthly mean soil moisture of CMIP5 used in this study is the water mass in all phases in the top 10 cm layer (kg/m^2) [*Taylor et al.*, 2012]. We used the outputs from 30 CMIP5 ESMs in the historical experiment, and 27 models in the RCP4.5 and RCP8.5 experiments (Table 1). The first ensemble run was used if a model had multiple ensemble simulations, so the effect of "model structure" was estimated by contrasting different model simulations. As the models have different spatial resolutions, ranging from 0.94° to 3.75°, all model outputs were bilinearly interpolated to a 1° latitude × 1° longitude grid to allow various diagnostics to be carried out across the models and matched to those of the GLDAS data. We selected the period 1920 – 2005 for the historical simulations and the period 2006 – 2080 for the RCP projections for our calculations and analyses.

2.2 CESM outputs

The CESM is an ESM consisting of atmosphere, land, ocean, and sea ice components that are linked through a coupler for exchanging state information and fluxes among these components [*Hurrell et al.*, 2013]. Two model simulations, the CESM Large Ensemble Project and Medium Ensemble Project, were used in this study. The CESM Large Ensemble

Project is a community resource for studying climate change in the presence of natural climate variability using historical forcing from 1920 to 2005, and then the RCP8.5 forcing scenario from 2006 to 2080 [*Kay et al.*, 2015]. The CESM Large Ensemble Project includes 30 ensemble perturbation simulations, so the effects of "initial conditions" can be estimated by contrasting the ensemble members. All 30 CESM Large Ensemble Project members use the same model and the same external forcing. The horizontal resolution is $0.94° \times 1.25°$ (latitude by longitude). The CESM Medium Ensemble Project uses the same strategies as the Large Ensemble Project but with a smaller ensemble size of 15; furthermore, it is forced by the RCP4.5 scenario [*Lin et al.*, 2016; *Sanderson et al.*, 2015]. The simulated soil moisture fields of CESM include 15 vertical layers from the surface to the bottom at 35 m (below the surface). In view of the comparability of different layers, we used the top soil moisture, and changed the unit of soil moisture to kg/m^2.

2.3 GLDAS data

Due to the lack of high-quality observational soil moisture data, the dataset from GLDAS was used to evaluate simulated soil moisture in the historical simulations over the global terrestrial surface. GLDAS is a global, high-resolution, offline land data assimilation system, which can generate optimal fields of land surface states and flux by integrating satellite- and ground-based observational data products, using land surface modeling and data assimilation techniques [*Rodell et al.*, 2004]. The GLDAS dataset was validated against available data taken from multiple sources [*Chen et al.*, 2013; *Dorigo et al.*, 2012; *Zhang et al.*, 2008]. We also validated the accuracy of GLDAS soil moisture by comparing it with observations in China (See Figure S1, S2, S3 and the content in the supplementary materials). It is widely

used for data assimilation, validation, weather and climate model initialization, and hydrology [*Cheng et al.*, 2015; *Cheng and Huang*, 2016; *Lin et al.*, 2008; *Reichle et al.*, 2007; *Yang et al.*, 2009]. The soil moisture data used in this study were the soil moisture contents in the top 10 cm layer (water mass in all phases, kg/m^2), taken from the monthly GLDAS Version 2 from 1948 to 2010 (spatial resolution, $1° \times 1°$). The GLDAS Version 2 product is a simulation outputs from the National Centers for Environmental Prediction/Oregon State University/Air Force/Hydrologic Research Lab (Noah) [*Chen and Dudhia*, 2001; *Chen et al.*, 1997; *Chen et al.*, 1996; *Ek et al.*, 2003] land surface model, forced with the Princeton meteorological dataset [*Sheffield et al.*, 2006].

2.4 Methods

The statistical methods used in this study were correlation analysis, regression analysis, wavelet analysis, and ensemble empirical mode decomposition (EEMD). EEMD separates non-uniform variability at different time scales [*Huang et al.*, 1998]. In EEMD, time series is decomposed to obtain a set of intrinsic mode functions (IMFs), which are a series of amplitude-frequency-modulated oscillatory components. The last IMF, either a monotonic curve or containing only one extremum, can be recognized as the trend of the time series. This trend has low sensitivity to the addition of new data. This property guarantees that the physical interpretation within a specified time interval does not change with the addition of new data, consistent with the physical constraint that the subsequent evolution of a physical system cannot alter what has already occurred. EEMD has been widely applied in climate research [*Ji et al.*, 2014; *Wu et al.*, 2011]. In the EEMD calculation for this study, the noise added to data had an amplitude of 0.2 standard deviations relative to the corresponding data,

the ensemble number was 400, and the number of IMFs was 6.

3. Results

3.1 Historical simulations (1920 – 2005)

Both CMIP5 and CESM experiments provided a suite of historical simulations with different ESMs or initial conditions. An ensemble mean is normally used to reduce model deviation. Figure 1 shows the global distributions of annual mean soil moisture during the period 1961 – 1990, namely the ensemble means of CMIP5 (CMIP5-EM; Figure 1a) and CESM simulations (CESM-EM; Figure 1b). For comparison, we also present the soil moisture distribution from GLDAS data (Figure 1c). High-latitude areas (poleward of 60°S or 70°N) are ignored, because they are dominated by permafrost. As shown in Figure 1, the simulated soil moisture broadly agrees with the GLDAS data, ranging from less than 10 kg/m^2 to a maximum of more than 35 kg/m^2. The driest regions are located in the Sahara and Arabian Peninsula, followed by the Iranian Plateau, western China, and western Australia. The wettest regions are mainly distributed in the tropics, especially 10°N – 10°S, such as the Amazon Basin and Congo Basin. The distribution of soil moisture is broadly comparable with precipitation characteristics but with some regional differences. This indicates that soil moisture depends mainly on precipitation, but precipitation is not the only controlling factor. CMIP5-EM underestimates soil moisture (relative to the GLDAS data) over most regions. In contrast, the CESM-EM is remarkably similar to the GLDAS data over most areas but largely underestimates soil moisture over northern Eurasia. The discrepancy for individual CMIP5 simulations is larger than that for individual CESM simulations. All regions show standard

deviation of less than 10% for ensemble mean soil moisture in the CESM simulations. In contrast, all of the regions in the CMIP5 simulations show standard deviation larger than 10% for ensemble mean soil moisture, and 24.1% of the global land area show standard deviation larger than 40% (Figure S4). The most pronounced distinction occurred over the Sahara, Arabian Peninsula, Iranian Plateau, and western Australia, for which soil moisture ranges show the poorest agreement in dry regions.

Global annual mean soil moisture levels in the period 1961 – 1990 for individual CMIP5 ESMs, CESM simulations, and GLDAS data are presented in Figure 2. The discrepancy among the 30 CESM simulations is negligible, so only their ensemble mean is presented. Figure 2 shows the global annual mean soil moisture in CMIP5-EM, CESM-EM, and GLDAS, with values of 20.0 kg/m^2, 20.5 kg/m^2, and 22.1 kg/m^2, respectively. However, there are large differences in the magnitude of climatological soil moisture between different CMIP5 ESMs, ranging from 8.5 kg/m^2 to 26.1 kg/m^2. The maximum soil moisture was approximately triple the minimum value in these ESMs. This large difference means that users cannot simply apply the soil moisture from one product to other models. In fact, previous research emphasized that the true information of modeled soil moisture lies not in its absolute magnitude but in its variation over time, because soil moisture climatology varies greatly among models, and models have different operating ranges for soil moisture [*Dirmeyer et al.*, 2004]. Therefore, soil moisture anomaly (SMA) was calculated to eliminate the influence of large differences in absolute magnitude. The SMA in the study is the annual mean soil moisture anomaly relative to the base of averaged soil moisture for 30 years (average of annual mean soil moisture in the period of 1961 – 1990). Note that the SMA in

Figure 3 is monthly mean SMA, after removing the average of 12 months.

When considering the total monthly SMA (Figure 3), there is agreement on the profiles of SMA between the simulations of different ESMs. In addition, CMIP5-EM, CESM-EM, and GLDAS show good agreement. All of the time series show higher soil moisture values in winter, and lower values in summer and fall, in agreement with the seasonal cycle of the global Aridity Index [*Lin et al.*, 2015]. The climatological evolution of SMA in CMIP5-EM is dominated by an annual cycle, with a maximum (1.5 kg/m^2) in January and a minimum (–2.0 kg/m^2) in August, and an annual range of 3.5 kg/m^2. Nevertheless, there are distinct differences in the dynamic range of monthly variability. In eight out of the 30 simulations, soil moisture shows a large difference between dry and wet months with a standard deviation larger than 2 kg/m^2, while the rest 22 simulations show narrow ranges. The seasonal amplitude is much larger for the eight simulations, i.e., at least twice of that for the rest 22 simulations. The largest discrepancies between the two cases occur in July and August, when the soil moisture content is low. Despite these differences, the evolution of SMA among individual simulations is highly consistent, and therefore the annual mean SMA is used hereafter.

The temporal variation of annual mean SMA (relative to the baseline period of 1961 – 1990) of CMIP5-EM (from 1920 to 2005), CESM-EM (from 1920 to 2005), and GLDAS (from 1948 to 2010) are illustrated in Figure 4. One standard deviation is used to measure the differences between the ensemble members for the CMIP5 and CESM simulations. As the internal variability of the ensemble mean soil moisture has been removed, GLDAS is the 20-year running mean. The time series of annual mean SMA shows an observable downward

trend during the 86-year period of CMIP5-EM, at a rate of –0.0084 kg/m^2 per 10 year, which

significantly exceeds the 95% confidence level. In comparison, the long-term trend of

CESM-EM is not significant. Focusing on the period 1948 – 2005, there were significant

decreasing trends in both CMIP5-EM (at a rate of –0.012 kg/m^2 per 10 year at the 95%

confidence level) and GLDAS (at a rate of –0.0074 kg/m^2 per 10 year at the 95% confidence

level). However, CESM-EM showed an increasing trend, at a rate of 0.0037 kg/m^2 per 10

year, which was opposite to the drying characteristics revealed by the Palmer Drought

Severity Index [*Dai*, 2011] and the Aridity Index [*Huang et al.*, 2016b]. Despite the opposite

long-term trend, there were significant relationships between CMIP5-EM and CESM-EM

simulations (r = 0.33, is calculated between the two detrended time series, with significant

correlation at the 95% confidence level) for the period 1920 – 2005 at interannual to decadal

time scales. The SMAs of CMIP5-EM and CESM-EM showed similarly significant decreases

before 1953 (minimal value for the EEMD IMF6 of CESM-EM), at rates of –0.014 kg/m^2 per

10 year and – 0.017 kg/m^2 per 10 year, respectively; these rates significantly exceeded the 95%

confidence level. Since then, the long-term results became different: CMIP5-EM decreased,

and CESM-EM increased. The standard deviations for CMIP5 and CESM are also presented

in Figure 4b, and show a large range from 0.086 to 0.19 kg/m^2 for CMIP5 (from 0.073 to

0.16 kg/m^2 for CESM). The standard deviations for both CMIP5 and CESM showed obvious

year-to-year variability, but their long-term variability was different. The long-term

variability of the standard deviation for the CESM simulation showed an upward trend over

the 86-year period at the 95% confidence level. In comparison, the long-term variability of

the standard deviation for the CMIP5 was not significant, despite a decreasing trend over the

entire time span. However, the long-term variability of the standard deviation for the CMIP5 can be divided into two periods: rapid decrease before 1980, followed by an increase.

Above shows the climatology and average value of soil moisture, but changes in soil moisture are generally of interest. Figure 5 shows the spatial distributions of annual mean SMA trends for the period 1948 – 2005 for CMIP5-EM (a), CESM-EM (b), and GLDAS (c). Significant trends (p = 0.05) can be observed for 29.4% of the global land area based on the GLDAS soil moisture. Of the 29.4%, 53.1% was negative and 46.9% positive. The most prominent drying trends occurred in the Sahel, East Asia, eastern Australia, and western Europe. Many strong drying trends occurred in regions that already had relatively low average soil moisture values. We observed subtle wetting trends in central USA, eastern Europe, and western Australia. The soil moisture trend was broadly comparable with various drought indices, such as the Palmer Drought Severity Index [*Dai*, 2011; 2013; *Wang et al.*, 2014] and the Aridity Index [*Feng and Fu*, 2013; *Huang et al.*, 2016a; *Li et al.*, 2014], suggesting that the broad patterns exhibited by the GLDAS soil moisture data are likely reliable. In comparison with the GLDAS SMA trend, however, the magnitudes of CMIP5-EM and CESM-EM SMA trends were much smaller. Focusing on the spatial distribution without considering the magnitude, the SMA trend of CMIP5-EM is remarkably similar to that of CESM-EM. The most prominent drying trends occurred in southern USA, northern South America, Europe, and Southeast Asia, and subtle wetting trends were seen in central Africa and western Asia. The spatial distributions were quite different from those of the GLDAS, especially in regions with prominent drying trends. This demonstrates that although the CMIP5 and CESM simulation can efficiently describe the spatial and temporal distributions

of global soil moisture, these models do not accurately reproduce regional soil moisture variation. Figure 5 also shows that the consistency of different CESM simulations is higher than that of the CMIP5 simulations. Stippling indicates that more than 80% (24 out of 30) of the simulations agree on the sign (positive or negative) of the change. Consistent changes were observed for 25.8% of the global land area for the CESM simulations, but the value was only 1.6% for the CMIP5 simulations. This demonstrates that model structure has a larger influence on soil moisture trend than initial conditions.

To express quantitatively the uncertainties in model structure and initial conditions at each grid point, relative standard deviation of SMA for the CMIP5 and CESM simulations, for the period 1920 – 2005 are calculated, and illustrated in Figure 6. Relative standard deviation in this study is defined as the ratio of standard deviation to mean soil moisture. It is better than commonly used standard deviation for expressing uncertainty of soil moisture, because it can eliminate the influence of different climatic conditions and allow comparison among different climatic regions. Figure 6a shows high values in the Sahara, Arabian Peninsula, the Iranian Plateau, northern China, and western Australia, indicating that these areas are most sensitive to climate model structure. In comparison with the CMIP5 simulations, the relative standard deviation of the CESM simulations exhibit similar spatial patterns (Figure 6b). The relative standard deviation values of CESM simulations are slightly larger than those of the CMIP5 over most regions, but the CMIP5 value for the Sahara is markedly larger than that for the CESM simulations. As the relative standard deviation depends largely on the climatic region, as shown in Figure 6a and Figure 6b, the regionally averaged relative standard deviation, as a function of climatological mean soil moisture, are

presented in Figure 6c. The climatological mean soil moisture is the annual mean soil moisture for the period 1961 – 1990, which represents the climatological state. The relative standard deviation decreases with the increase in climatological mean soil moisture. This indicates that the SMA agrees best in humid areas. Figure 6c is also a visual performance of the comparison between CMIP5 and CESM simulations in different climatic regions, which shows large model structure uncertainty in very dry regions, but a slightly larger initial uncertainty in other regions.

Although the quantitative uncertainty was analyzed by standard deviation and relative standard deviation in Figure 4 and Figure 6, standard deviation can only reflect the deviation between the individual models or simulations. Temporal consistency of long-term and interannual variability cannot be revealed by standard deviation. Standard deviation is a state average, which may neglect some important details. Figure 7 shows the time series of annual mean SMA for the period 1920 – 2005, for 30 individual members of the CMIP5 and of CESM simulations, which shows large differences among the members. Of these 30 CMIP5 simulations, 22 members show decreasing trends (13 of them are significant at the 95% confidence level), and eight show increasing trends (three of them are significant at the 95% confidence level). However, for the CESM simulations, only two members show significant decreasing trends and one member shows a significant increasing trend. Although the individual simulations show large variability at interannual to decadal time scales, the ensemble mean only shows a low-frequency signal. The averaged standard deviation for the individual members of the CMIP5 (CESM) is 0.13 (0.12) kg/m^2, but the standard deviation for CMIP5-EM (CESM-EM) is 0.038 (0.030) kg/m^2. This indicates that the ensemble mean

can effectively remove the uncertainty in internal variability.

To study the uncertainty at different time scales, the EEMD was used to separate non-uniform variability at different timescales for the CMIP5 and CESM SMA. Figure 8 shows the time series of EEMD IMF1 to IMF6 in the period 1920 – 2005, for 30 individual members of the CMIP5 and CESM simulations. IMF6 can be recognized as a linear trend in the time series, and IMF1 to IMF5 are the signals of SMA from high to low frequency. The highest cycle powers for IMF1 to IMF5 are $3 - 5$, $7 - 10$, $14 - 20$, $40 - 45$, and 78 years, as detected by wavelet analysis using the Morlet wavelet. IMF1 mainly reflects the periodic signal at the interannual time scale. The standard deviation for IMF1 of CMIP5 ranges from 0.062 to 0.13 (from 0.066 to 0.11 for CESM) with temporal variability. IMF6 shows the linear trend of the time series. We determined the increment of the EEMD trend at a given time from the reference time of 1920, i.e., $Trend_{EEMD}(t) = IMF6(t) - IMF6(1920)$, representing the accumulated trend from 1920 [*Ji et al.*, 2014]. $Trend_{EEMD}(2005)$ can be recognized as the trend of the SMA series from 1920 to 2005. Of these 30 CMIP5 simulations, 22 members show a decreasing trend and eight members show an increasing trend, which is markedly consistent with the linear trend. Of these 30 CESM simulations, 21 members show a decreasing trend, and nine members show an increasing trend. Same as IMF1 and IMF6, large difference also exists for IMF2 to IMF5, which indicate that both model structure and initial conditions can cause uncertainty at all time scales. Comparing the ensemble mean with its individual simulations, we find that the fluctuation of the ensemble mean is much smaller than the individual simulations for all of the IMFs. This indicates that the ensemble mean can not only effectively removes the fluctuations in internal variability, but also the signal at

interdecadal time scales, which are sometimes useful and important. Therefore, using ensemble mean is not entirely appropriate under these circumstances.

3.2 Future projections (2006 – 2080) forced by RCPs

Using similar analysis for historical simulations, the uncertainties of future projections (2006 – 2080) under RCP4.5 and RCP8.5 are also presented. Figure 9 shows the time series of annual mean SMA in the period 2006 – 2080, relative to the period 2006 – 2025, for 27 CMIP5 and 30 CESM simulations. The shaded area is one standard deviation. The gray lines show the 20-year moving averages of 30 individual members, and the black lines show the averaged values. The ensemble mean SMA clearly shows projected 21st century changes. There is a downward trend during the projected 21st century for CMIP5 RCP4.5 (RCP8.5), at a rate of –0.045 (–0.074) kg/m^2 per 10 year, which significantly exceeds the 95% confidence level for both scenarios. In comparison with the CMIP5, the ensemble mean SMA of the CESM simulation also shows a significant drying trend, at a rate of –0.026 (–0.044) kg/m^2 per 10 year for RCP4.5 (RCP8.5). For the period 2061 – 2080, the CMIP5 (CESM) model simulations show ensemble mean decrease in annual mean SMA, of –0.25 (–0.14) kg/m^2 for RCP4.5 and – 0.40 (–0.25) kg/m^2 for RCP8.5, respectively, relative to the period 2006 – 2025. Almost all of the CMIP5 and CESM individual simulations show a significant linear decreasing trend for the 21st century, although large differences exist among these trends.

The time series of standard deviation of annual mean SMA for the CMIP5 and CESM simulations in the period 2006 – 2080 are presented in Figure 10, showing significant increasing trends. The trends were 0.017, 0.037, 0.0058, and 0.0060 kg/m^2 per 10 year for

CMIP5 RCP4.5, CMIP5 RCP8.5, CESM RCP4.5, and CESM RCP8.5, respectively. The results indicate that the uncertainties in model structure and initial conditions show an increasing trend in the future period. The standard deviations for the four sets of simulations show no significant difference before 2045, but subsequently become significantly different. For the period 2046 – 2080, the CESM simulations change little, at rates of 0.0073 and 0.0035 kg/m^2 per 10 year for RCP4.5 and RCP8.5, respectively, which are not significant. However, for the CMIP5 simulations, the rates are 0.016 and 0.068 kg/m^2 per 10 year for RCP4.5 and RCP8.5, respectively, which significantly exceeds the 95% confidence level. The spatial distributions of averaged relative standard deviation of SMA in the period 2006 – 2080 are remarkably similar to those of the historical simulations, which shows large uncertainties in the dry regions (Figure S5 and Figure S6). The relative standard deviation for RCP8.5 is slightly larger than that for RCP4.5, although the difference is not significant (Figure S5 and Figure S6). This indicates that the uncertainties of greenhouse gas emission scenarios are smaller than the uncertainties of model structure and initial conditions.

Based on the analysis of soil moisture uncertainty, Figure 11 shows percentage changes in soil moisture for the 20-year period 2061 – 2080 relative to the period 2006 – 2025. Stippling indicates that more than 80% of the models agree on the sign of change (positive or negative). The broad patterns are consistent across the RCPs, with stronger changes for RCP8.5. Under RCP8.5 of CMIP5, 22.3% of the global land area shows consistent soil moisture changes across individual ensemble members. Of these, 98.3% shows drying and 1.7% wetting. The most prominent drying change occurs in the Mediterranean region, northeast and southwest South America, southern Africa, and southwestern USA. The

multi-model mean suggests decreases larger than 4% by 2061 – 2080 in these regions. The agreement among CMIP5 models indicates high confidence in certain regions where surface soils are projected to dry. The large-scale drying in these regions is likely caused by various processes, such as the widening of the Hadley circulation and global temperature warming [*Stocker et al.*, 2013]. However, ensemble members show disagreement in terms of the sign of change in Asia, central Africa, and northern USA. In addition, the drying in the soil moisture field of CMIP5 is largely reproduced by the CESM simulations, although the CESM results suggest larger increase in wetness over Southeast Asia and central Africa (Figure 11b and Figure 11d).

4. Summary and discussion

In this paper, the uncertainties of model structure and initial conditions of soil moisture were investigated using 30 CMIP5 ESMs and 30 CESM simulations. The results indicated that despite some disagreement, the simulated soil moisture broadly agrees with the GLDAS data in terms of spatial pattern, with the driest regions located in the Sahara, Arabian Peninsula, Iranian Plateau, western China, and western Australia, and the wettest regions distributed in the Amazon Basin and Congo Basin. However, the magnitude of climatological soil moisture varies enormously among different model simulations. In fact, the inconformity is largely unavoidable given the coarse model resolution and strong nonlinearity in the governing soil moisture–evaporation relationship [*Koster et al.*, 2009].

When eliminating the influence of large differences in absolute magnitudes, all of the individual simulations of monthly SMA showed higher values in winter and lower values in

summer and fall. Therefore, we analyzed the temporal variation of annual mean SMA of the CMIP5 and CESM during 1920 – 2005, which showed an observable downward trend in CMIP5-EM, and non-apparent long-term variability in CESM-EM. Significant decreasing trends for CMIP5-EM and GLDAS were observed in the period 1948 – 2005, while the opposite trend was seen in CESM-EM. Moreover, the spatial distributions of soil moisture trends in CMIP5-EM and CESM-EM were quite different from those in the GLDAS, especially for regions with prominent drying trends. An aspect of our findings that requires special attention is that although the GLDAS data were used to evaluate soil moisture in the historical simulations, GLDAS is not observation and the results are not faultless. To obtain a more accurate estimate, additional observations are needed.

The standard deviations of the CMIP5 and CESM outputs were used to express quantitative uncertainties of model structure and initial conditions. The results showed high uncertainties in the Sahara, Arabian Peninsula, Iranian Plateau, northern China, and western Australia, which had relatively low average soil moisture values. The uncertainty of initial conditions is slightly larger than the uncertainty of model structure, except for the very dry regions. The uncertainty in initial conditions showed an upward long-term trend during the 86-year period, but the long-term variability in model structure uncertainty for the same period is not significant, due to two opposite trends: a rapid decrease before 1980 followed by a subsequent increase. When separating the time series of SMA by EEMD analysis, the results indicated that model structure and initial conditions can cause uncertainties at all time scales.

The uncertainties of future projections (2006 – 2080) under RCP4.5 and RCP8.5 were

also presented, and demonstrated similar spatial distributions of uncertainties to those of the historical simulations. In addition, the uncertainties in model structure and initial conditions showed an increasing trend in the period 2006 – 2080, especially for CMIP5 RCP8.5. In contrast to the inconsistent long-term variability of historical simulations, almost all of the CMIP5 and CESM individual simulations showed significant linear decreasing trends for the 21st century. In addition, the most prominent drying trends occurred in the Mediterranean region, northeast and southwest South America, southern Africa, and southwestern USA. Despite similar drying trends among the individual simulations, the degree of soil moisture drying is debatable due to large uncertainty.

For CESM data requests, please contact the corresponding author (hjp@lzu.edu.com).

References

Ahlström, A., G. Schurgers, A. Arneth, and B. Smith (2012), Robustness and uncertainty in terrestrial ecosystem carbon response to CMIP5 climate change projections, *Environ. Res. Lett.*, *7*(4), 044008, doi:10.1088/1748-9326/7/4/044008.

Aloysius, N. R., J. Sheffield, J. E. Saiers, H. Li, and E. F. Wood (2016), Evaluation of historical and future simulations of precipitation and temperature in central Africa from CMIP5 climate models, *J. Geophys. Res.: Atmos.*, *121*(1), 130-152, doi:10.1002/2015JD023656.

Bracegirdle, T. J., J. Turner, J. S. Hosking, and T. Phillips (2014), Sources of uncertainty in projections of twenty-first century westerly wind changes over the Amundsen Sea, West Antarctica, in CMIP5 climate models, *Clim. Dyn.*, *43*(7), 2093-2104, doi:10.1007/s00382-013-2032-1.

Chen, F., and J. Dudhia (2001), Coupling an advanced land surface-hydrology model with the Penn State-NCAR MM5 modeling system. Part I: Model implementation and sensitivity, *Mon. Weather Rev.*, *129*(4), 569-585, doi: 10.1175/1520-0493(2001)129<0569:CAALSH>2.0.CO;2.

Chen, F., Z. Janjić, and K. Mitchell (1997), Impact of atmospheric surface-layer parameterizations in the new land-surface scheme of the NCEP mesoscale Eta model, *Bound-lay Meteorol.*, *85*(3), 391-421, doi:10.1023/A:1000531001463.

Chen, F., K. Mitchell, J. Schaake, Y. Xue, H. Pan, V. Koren, Q. Duan, M. Ek, and A. Betts (1996), Modeling of land surface evaporation by four schemes and comparison with FIFE observations, *J. Geophys. Res.: Atmos.*, *101*(D3), 7251-7268, doi:10.1029/95JD02165.

Chen, Y., K. Yang, J. Qin, L. Zhao, W. Tang, and M. Han (2013), Evaluation of AMSR-E retrievals and GLDAS simulations against observations of a soil moisture network on the central Tibetan Plateau, *J. Geophys. Res.: Atmos.*, *118*(10), 4466-4475, doi:10.1002/jgrd.50301.

Cheng, S., X. Guan, J. Huang, F. Ji, and R. Guo (2015), Long-term trend and variability of soil moisture over East Asia, *J. Geophys. Res.: Atmos.*, *120*(17), 8658-8670, doi:10.1002/2015JD023206.

Cheng, S., and J. Huang (2016), Enhanced soil moisture drying in transitional regions under a warming climate, *J. Geophys. Res.: Atmos.*, *121*, doi:doi:10.1002/2015JD024559.

Ciais, P., et al. (2005), Europe-wide reduction in primary productivity caused by the heat and drought in 2003, *Nature*, *437*(7058), 529-533, doi:10.1038/nature03972.

Cook, B. I., G. B. Bonan, and S. Levis (2006), Soil moisture feedbacks to precipitation in southern Africa, *J. Climate*, *19*(17), 4198-4206, doi:10.1175/JCLI3856.1.

Dai, A. (2011), Drought under global warming: A review, *WIRES. Clim. Change*, *2*(1), 45-65, doi:10.1002/wcc.81.

Dai, A. (2013), Increasing drought under global warming in observations and models, *Nat. Clim. Change*, *3*(1), 52-58, doi:10.1038/nclimate1633.

Dirmeyer, P. A., X. Gao, M. Zhao, Z. Guo, T. Oki, and N. Hanasaki (2006), GSWP-2: Multimodel analysis and implications for our perception of the land surface, *B. Am. Meteorol. Soc.*, *87*(10), 1381-1397, doi:10.1175/BAMS-87-10-1381.

Dirmeyer, P. A., Z. Guo, and X. Gao (2004), Comparison, validation, and transferability of eight multiyear global soil wetness products, *J. Hydrometeorol.*, *5*(6), 1011-1033, doi:10.1175/JHM-388.1.

Dorigo, W., R. Jeu, D. Chung, R. Parinussa, Y. Liu, W. Wagner, and D. Fernández-Prieto (2012), Evaluating global trends (1988–2010) in harmonized multi-satellite surface soil moisture, *Geophys. Res. Lett.*, *39*(18), L18405, doi:10.1029/2012GL052988.

Ek, M., K. Mitchell, Y. Lin, E. Rogers, P. Grunmann, V. Koren, G. Gayno, and J. Tarpley (2003),

Implementation of Noah land surface model advances in the National Centers for Environmental Prediction operational mesoscale Eta model, *J. Geophys. Res.: Atmos.*, *108*(D22), 8851, doi:10.1029/2002JD003296.

Feng, S., and Q. Fu (2013), Expansion of global drylands under a warming climate, *Atmos. Chem. Phys.*, *13*(19), 10081-10094, doi:10.5194/acp-13-10081-2013.

Findell, K. L., and E. A. Eltahir (2003a), Atmospheric controls on soil moisture-boundary layer interactions. Part I: Framework development, *J. Hydrometeorol.*, *4*(3), 552-569, doi:10.1175/1525-7541(2003)004<0552:ACOSML>2.0.CO;2.

Findell, K. L., and E. A. Eltahir (2003b), Atmospheric controls on soil moisture-boundary layer interactions. Part II: Feedbacks within the continental United States, *J. Hydrometeorol.*, *4*(3), 570-583, doi:10.1175/1525-7541(2003)004<0570:ACOSML>2.0.CO;2.

Guan, X., J. Huang, N. Guo, J. Bi, and G. Wang (2009), Variability of soil moisture and its relationship with surface albedo and soil thermal parameters over the Loess Plateau, *Adv. Atmos. Sci.*, *26*(4), 692-700, doi:10.1007/s00376-009-8198-0.

Huang, J., M. Ji, Y. Xie, S. Wang, Y. He, and J. Ran (2016a), Global semi-arid climate change over last 60 years, *Clim. Dyn.*, *46*(3), 1131-1150, doi:10.1007/s00382-015-2636-8.

Huang, J., H. Yu, X. Guan, G. Wang, and R. Guo (2016b), Accelerated dryland expansion under climate change, *Nat. Clim. Change*, *6*, 166-171, doi:10.1038/nclimate2837.

Huang, J., et al. (2008), An overview of the semi-arid climate and environment research observatory over the Loess Plateau, *Adv. Atmos. Sci.*, *25*(6), 906-921, doi:10.1007/s00376-008-0906-7.

Huang, N. E., Z. Shen, S. R. Long, M. C. Wu, H. H. Shih, Q. Zheng, N. Yen, C. C. Tung, and H. H. Liu (1998), The empirical mode decomposition and the Hilbert spectrum for nonlinear and non-stationary time series analysis, *Proc. R. Soc. London.*, *454*, 903 – 995.

Hurrell, J. W., et al. (2013), The community earth system model: a framework for collaborative research, *B. Am. Meteorol. Soc.*, *94*(9), 1339-1360, doi:10.1175/BAMS-D-12-00121.1.

Ji, F., Z. Wu, J. Huang, and E. P. Chassignet (2014), Evolution of land surface air temperature trend, *Nat. Clim. Change*, *4*(6), 462-466, doi:10.1038/nclimate2223.

Kay, J. E., et al. (2015), The Community Earth System Model (CESM) large ensemble project: A community resource for studying climate change in the presence of internal climate variability, *B. Am. Meteorol. Soc.*, *96*(8), 1333-1349, doi:10.1175/BAMS-D-13-00255.1.

Knutti, R., and J. Sedláček (2013), Robustness and uncertainties in the new CMIP5 climate model projections, *Nat. Clim. Change*, *3*(4), 369-373, doi:10.1038/nclimate1716.

Koster, R. D., Z. Guo, R. Yang, P. A. Dirmeyer, K. Mitchell, and M. J. Puma (2009), On the nature of soil moisture in land surface models, *J. Climate*, *22*(16), 4322-4335, doi:10.1175/2009JCLI2832.1.

Koster, R. D., and P. C. D. Milly (1997), The interplay between transpiration and runoff formulations in land surface schemes used with atmospheric models, *J. Climate*, *10*(7), 1578-1591, doi:10.1175/1520-0442(1997)010<1578:TIBTAR>2.0.CO;2.

Kusunoki, S., and O. Arakawa (2015), Are CMIP5 Models Better than CMIP3 Models in Simulating Precipitation over East Asia?, *J. Climate*, *28*(14), 5601-5621, doi:10.1175/JCLI-D-14-00585.1.

Li, B., M. Rodell, B. F. Zaitchik, R. H. Reichle, R. D. Koster, and T. M. van Dam (2012), Assimilation of GRACE terrestrial water storage into a land surface model: evaluation and potential value for drought monitoring in western and central Europe, *J. Hydrol.*, *446*, 103-115, doi:10.1016/j.jhydrol.2012.04.035.

Li, Y., J. Huang, M. Ji, and J. Ran (2014), Dryland expansion in northern China from 1948 to 2008, *Adv. Atmos. Sci.*, *32*(6), 870-876, doi:10.1007/s00376-014-4106-3.

Lin, B., P. W. Stackhouse, P. Minnis, B. A. Wielicki, Y. Hu, W. Sun, T. F. Fan, and L. M. Hinkelman (2008),

Assessment of global annual atmospheric energy balance from satellite observations, *J. Geophys. Res.: Atmos.*, *113*(D16), D16114, doi:10.1029/2008JD009869.

Lin, L., A. Gettelman, S. Feng, and Q. Fu (2015), Simulated climatology and evolution of aridity in the 21st century, *J. Geophys. Res.: Atmos.*, *120*(12), 5795-5815, doi:10.1002/2014JD022912.

Lin, L., A. Gettelman, Q. Fu, and Y. Xu (2016), Simulated differences in 21st century aridity due to different scenarios of greenhouse gases and aerosols, *Climatic. Change*, 1-16, doi:10.1007/s10584-016-1615-3.

Orlowsky, B., and S. I. Seneviratne (2013), Elusive drought: uncertainty in observed trends and short-and long-term CMIP5 projections, *Hydrol. Earth. Syst. Sci.*, *17*(5), 1765-1781, doi:10.5194/hess-17-1765-2013.

Reichle, R. H., R. D. Koster, P. Liu, S. P. Mahanama, E. G. Njoku, and M. Owe (2007), Comparison and assimilation of global soil moisture retrievals from the Advanced Microwave Scanning Radiometer for the Earth Observing System (AMSR-E) and the Scanning Multichannel Microwave Radiometer (SMMR), *J. Geophys. Res.: Atmos.*, *112*(D9), D09108, doi:10.1029/2006JD008033.

Reichstein, M., et al. (2007), Reduction of ecosystem productivity and respiration during the European summer 2003 climate anomaly: a joint flux tower, remote sensing and modelling analysis, *Global. Change. Biol.*, *13*(3), 634-651, doi:10.1111/j.1365-2486.2006.01224.x.

Rodell, M., et al. (2004), The global land data assimilation system, *B. Am. Meteorol. Soc.*, *85*(3), 381-394, doi:10.1175/BAMS-85-3-381.

Sanderson, B. M., K. W. Oleson, W. G. Strand, F. Lehner, and B. C. O'Neill (2015), A new ensemble of GCM simulations to assess avoided impacts in a climate mitigation scenario, *Climatic. Change*, 1-16, doi:10.1007/s10584-015-1567-z.

Seneviratne, S. I., T. Corti, E. L. Davin, M. Hirschi, E. B. Jaeger, I. Lehner, B. Orlowsky, and A. J. Teuling (2010), Investigating soil moisture–climate interactions in a changing climate: A review, *Earth sci. Rev.*, *99*(3), 125-161, doi:10.1016/j.earscirev.2010.02.004.

Sheffield, J., G. Goteti, and E. Wood (2006), Development of a 50-year high-resolution global dataset of meteorological forcings for land surface modeling, *J. Climate,*, *19*(13), 3088-3111, doi:10.1175/JCLI3790.1.

Sheffield, J., and E. F. Wood (2008), Global trends and variability in soil moisture and drought characteristics, 1950-2000, from observation-driven simulations of the terrestrial hydrologic cycle, *J. Climate*, *21*(3), 432-458, doi:10.1175/2007JCLI1822.1.

Stocker, T. F., D. Qin, G.-K. Plattner, M. Tignor, S. K. Allen, J. Boschung, A. Nauels, Y. Xia, V. Bex, and P. M. Midgley (2013), *IPCC, 2013: Climate change 2013: The physical science basi,* Cambridge Univ. Press, Cambridge, U. K. and New York.

Taylor, K. E., R. J. Stouffer, and G. A. Meehl (2012), An overview of CMIP5 and the experiment design, *B. Am. Meteorol. Soc.*, *93*(4), 485-498, doi:10.1175/BAMS-D-11-00094.1.

Wagner, W., K. Scipal, C. Pathe, D. Gerten, W. Lucht, and B. Rudolf (2003), Evaluation of the agreement between the first global remotely sensed soil moisture data with model and precipitation data, *J. Geophys. Res.: Atmos.*, *108*(D19), 4611, doi:10.1029/2003JD003663.

Wang, G., J. Huang, W. Guo, J. Zuo, J. Wang, J. Bi, Z. Huang, and J. Shi (2010), Observation analysis of land-atmosphere interactions over the Loess Plateau of northwest China, *J. Geophys. Res.: Atmos.*, *115*(D7), D00K17, doi:10.1029/2009JD013372.

Wang, S., J. Huang, Y. He, and Y. Guan (2014), Combined effects of the Pacific Decadal Oscillation and El Niño-Southern Oscillation on Global Land Dry–Wet Changes, *Sci. Rep.*, *4*, 6651, doi:10.1038/srep06651.

Woldemeskel, F. M., A. Sharma, B. Sivakumar, and R. Mehrotra (2012), An error estimation method for precipitation and temperature projections for future climates, *J. Geophys. Res.: Atmos.*, *117*(D22), D22104,

doi:10.1029/2012JD018062.

Woldemeskel, F. M., A. Sharma, B. Sivakumar, and R. Mehrotra (2016), Quantification of precipitation and temperature uncertainties simulated by CMIP3 and CMIP5 models, *J. Geophys. Res.: Atmos.*, *121*(1), 3-17, doi:10.1002/2015JD023719.

Wu, Z., N. E. Huang, J. M. Wallace, B. V. Smoliak, and X. Chen (2011), On the time-varying trend in global-mean surface temperature, *Clim. Dyn.*, *37*(3), 759-773, doi:10.1007/s00382-011-1128-8.

Yang, K., T. Koike, I. Kaihotsu, and J. Qin (2009), Validation of a dual-pass microwave land data assimilation system for estimating surface soil moisture in semiarid regions, *J. Hydrometeorol*, *10*(3), 780-793, doi:10.1175/2008JHM1065.1.

Yang, K., T. Watanabe, T. Koike, X. Li, H. Fujii, K. Tamagawa, Y. Ma, and H. Ishikawa (2007), Auto-calibration system developed to assimilate AMSR-E data into a land surface model for estimating soil moisture and the surface energy budget, *J. Meteorol. Soc. Jpn.*, *85A*, 229-242.

Yang, Z., et al. (2011), The community Noah land surface model with multiparameterization options (Noah-MP): 2. Evaluation over global river basins, *J. Geophys. Res.: Atmos.*, *116*(D12), D12110, doi:10.1029/2010JD015140.

Zhang, J., W. C. Wang, and J. Wei (2008), Assessing land-atmosphere coupling using soil moisture from the Global Land Data Assimilation System and observational precipitation, *J. Geophys. Res.: Atmos.*, *113*(D17), D17119, doi:10.1029/2008JD009807.

Table 1. List of CMIP5 ESMs used in this study with brief descriptions. The symbols "H" and "R" in the experiments indicate the historical run (1920 – 2005) and two future scenario (RCP4.5 and RCP8.5) runs (2006 – 2080) used in this study. The first ensemble run is used if a model has multiple ensemble runs.

	Model Names	Experiments	Origin
1	bcc-csm1-1	H,R	Beijing Climate Center, China Meteorological Administration, China
2	bcc-csm1-1-m	H,R	Beijing Climate Center, China Meteorological Administration, China
3	BNU-ESM	H,R	College of Global Change and Earth System Science, Beijing Normal University, China
4	CanESM2	H,R	Canadian Centre for Climate Modelling and Analysis, Canada
5	CCSM4	H,R	National Center for Atmospheric Research, USA
6	CESM1-BGC	H,R	Community Earth System Model Contributors, USA
7	CESM1-CAM5	H	Community Earth System Model Contributors, USA
8	CESM1-FASTCHEM	H	Community Earth System Model Contributors, USA
9	CESM1-WACCM	H	Community Earth System Model Contributors, USA
10	CNRM-CM5-2	H	Centre National de Recherches Météorologiques / Centre Européen de Recherche et Formation Avancée en Calcul Scientifique, France
11	CNRM-CM5	H	Centre National de Recherches Météorologiques / Centre Européen de Recherche et Formation Avancée en Calcul Scientifique, France
12	GFDL-CM3	H,R	NOAA Geophysical Fluid Dynamics Laboratory, USA
13	GFDL-ESM2G	H,R	NOAA Geophysical Fluid Dynamics Laboratory, USA
14	GFDL-ESM2M	H,R	NOAA Geophysical Fluid Dynamics Laboratory, USA
15	GISS-E2-H-CC	H,R	NASA Goddard Institute for Space Studies, USA
16	GISS-E2-R-CC	H,R	NASA Goddard Institute for Space Studies, USA
17	GISS-E2-R	H,R	NASA Goddard Institute for Space Studies, USA
18	HadCM3	H	Met Office Hadley Centre, UK
19	HadGEM2-CC	H,R	Met Office Hadley Centre, UK
20	HadGEM2-ES	H,R	Met Office Hadley Centre, UK
21	IPSL-CM5A-LR	H,R	Institut Pierre-Simon Laplace, France
22	IPSL-CM5A-MR	H	Institut Pierre-Simon Laplace, France
23	IPSL-CM5B-LR	H,R	Institut Pierre-Simon Laplace, France
24	MIROC5	H,R	Atmosphere and Ocean Research Institute, Japan
25	MIROC-ESM-CHEM	H,R	Japan Agency for Marine-Earth Science and

			Technology, Japan
26	MIROC-ESM	H,R	Japan Agency for Marine-Earth Science and Technology, Japan
27	MRI-CGCM3	H,R	Meteorological Research Institute, Japan
28	MRI-ESM1	H	Meteorological Research Institute, Japan
29	NorESM1-ME	H	Norwegian Climate Centre, Norway
30	NorESM1-M	H	Norwegian Climate Centre, Norway
31	ACCESS1-0	R	Commonwealth Scientific and Industrial Research Organization (CSIRO) and Bureau of Meteorology (BOM), Australia
32	ACCESS1-3	R	CSIRO and BOM, Australia
33	CESM1-CAM5-1-FV2	R	Community Earth System Model Contributors, USA
34	CSIRO-Mk3-6-0	R	CSIRO in collaboration with Queensland Climate Change Centre of Excellence, Australia
35	FGOALS-g2	R	LASG, Institute of Atmospheric Physics, Chinese Academy of Sciences and CESS, Tsinghua University, China
36	GISS-E2-H	R	NASA Goddard Institute for Space Studies, USA
37	inmcm4	R	Institute for Numerical Mathematics, Russia
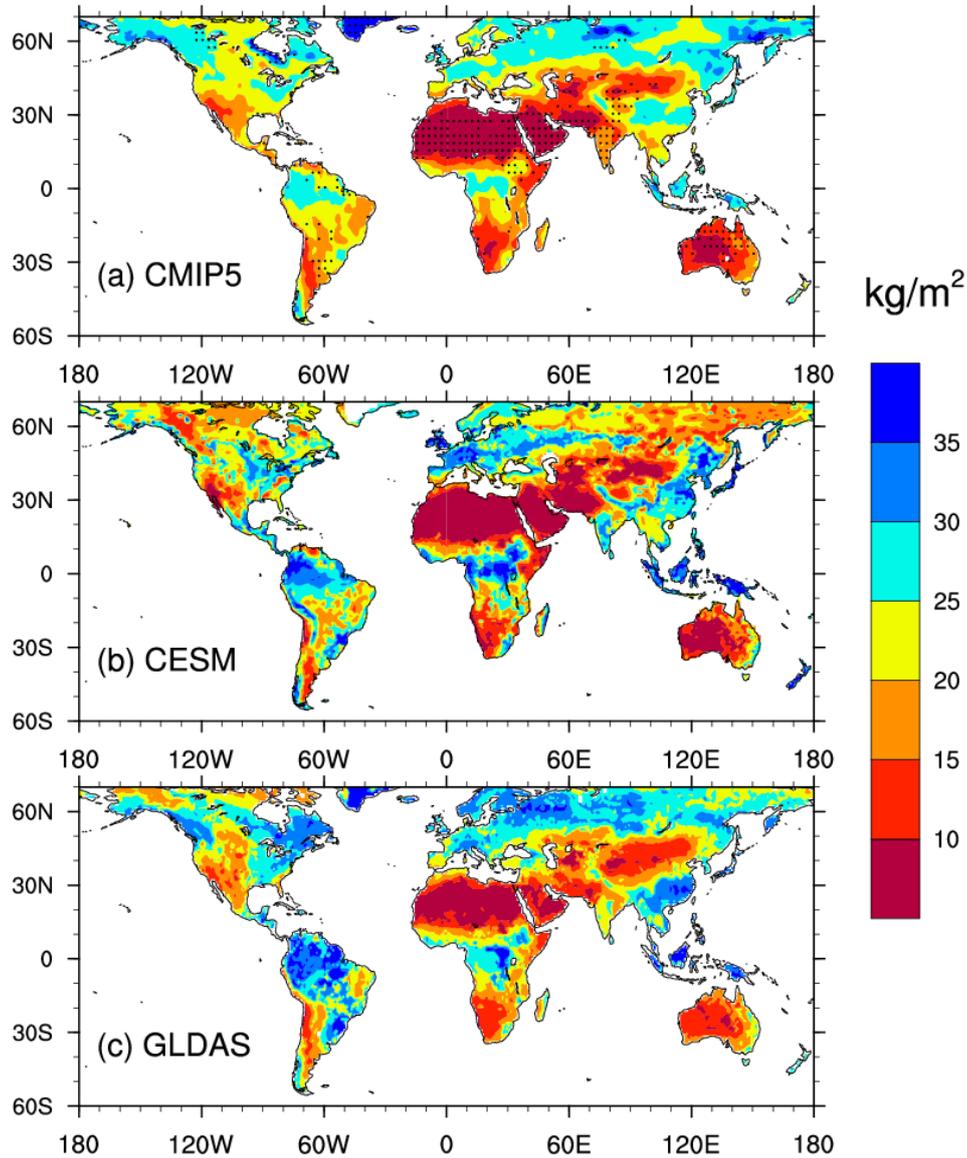
Figure 1. Spatial distributions of annual mean surface soil moisture in the period 1961 –
1990 for (a) ensemble mean of the Coupled Model Intercomparison Project Phase 5
(CMIP5-EM), (b) ensemble mean of the Community Earth System Model (CESM-EM) (b),
and (c) the Global Land Data Assimilation System (GLDAS). The stippling in (a) denotes
that the standard deviation is more than 40% of the ensemble mean soil moisture.
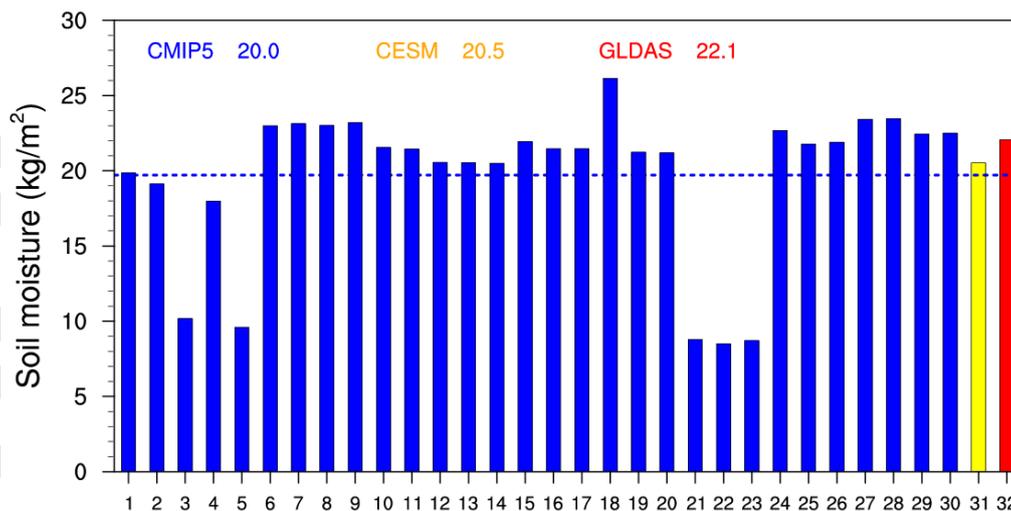
Figure 2. Global annual mean soil moisture in the period 1961 – 1990 for CMIP5 (Nos. 1 – 30), CESM-EM (31), and GLDAS (32). The dashed horizontal line is the average value of 30 CMIP5 Earth System Models (ESMs). The numbers of CMIP5 ESMs (1 – 30) are the same as those in Table 1. The discrepancies among the 30 CESM simulations are negligible, so we present their ensemble mean here. The numbers indicate their average values.
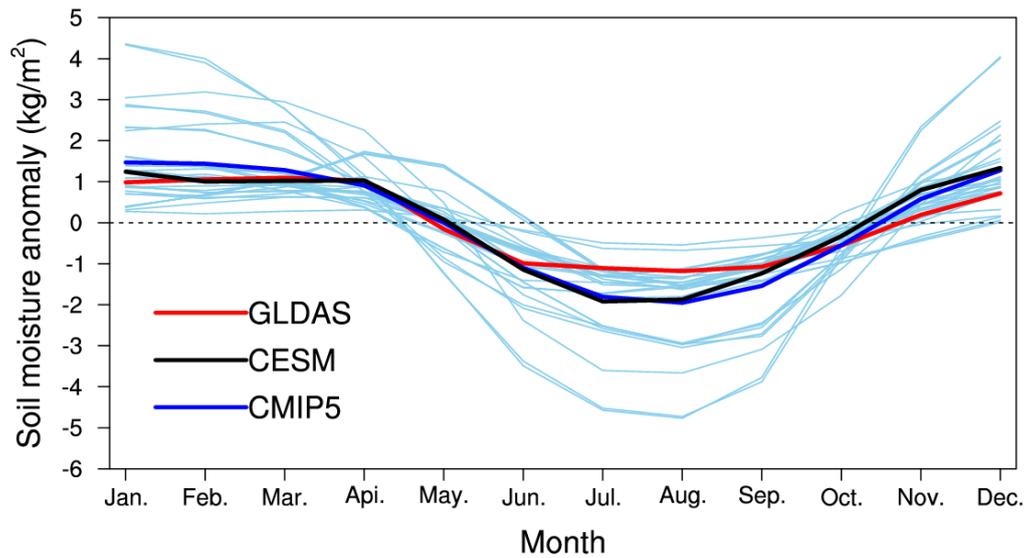
Figure 3. Global monthly mean soil moisture anomaly (SMA) for the period 1961 – 1990. The blue curve shows the CMIP5-EM, the thin blue curves show 30 individual CMIP5 simulations; the black curve shows the CESM-EM, and the red curve shows the GLDAS. The discrepancies for the 30 CESM simulations are negligible, so we present their ensemble mean here.
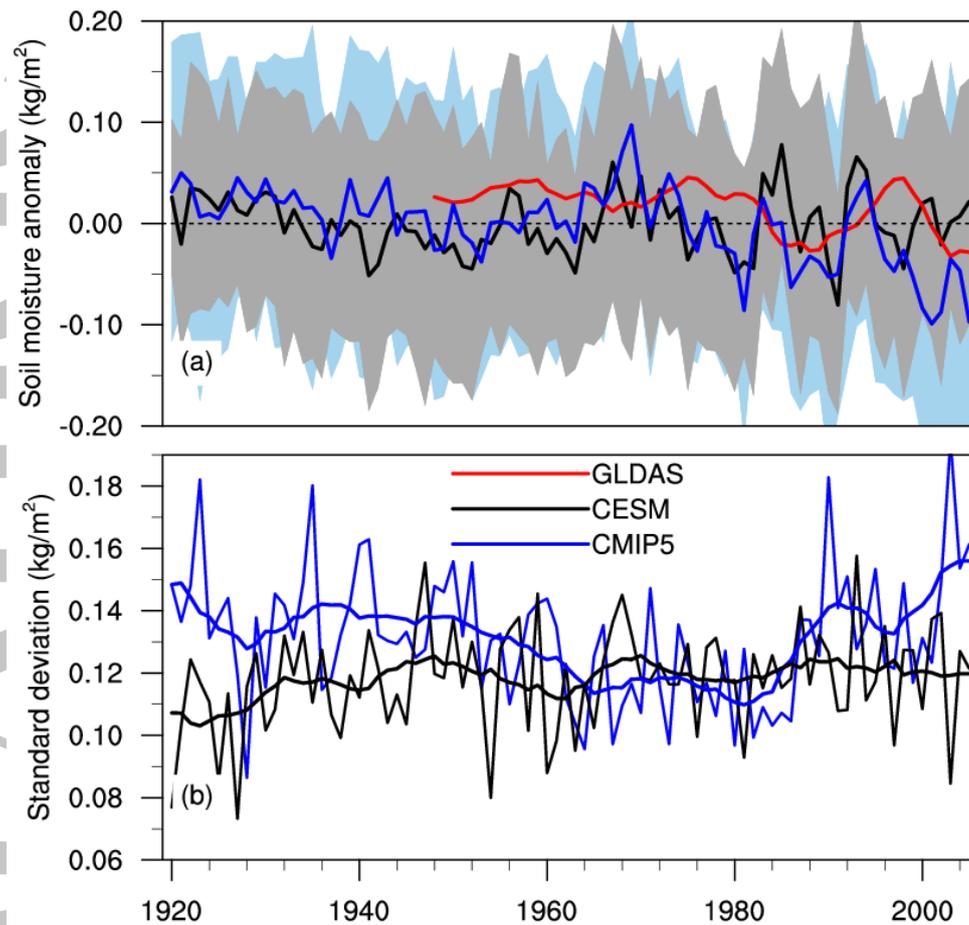
Figure 4. (a) Time series of annual mean SMA in the period 1920 – 2005 relative to the period 1961 – 1990 for the CMIP5-EM and CESM-EM. Uncertainty (shading) is one standard deviation. The red curve is the 20-year moving average of GLDAS soil moisture. (b) Time series and 10-year moving average of standard deviation of annual mean SMA for the CMIP5 and CESM in the period 1920 – 2005.
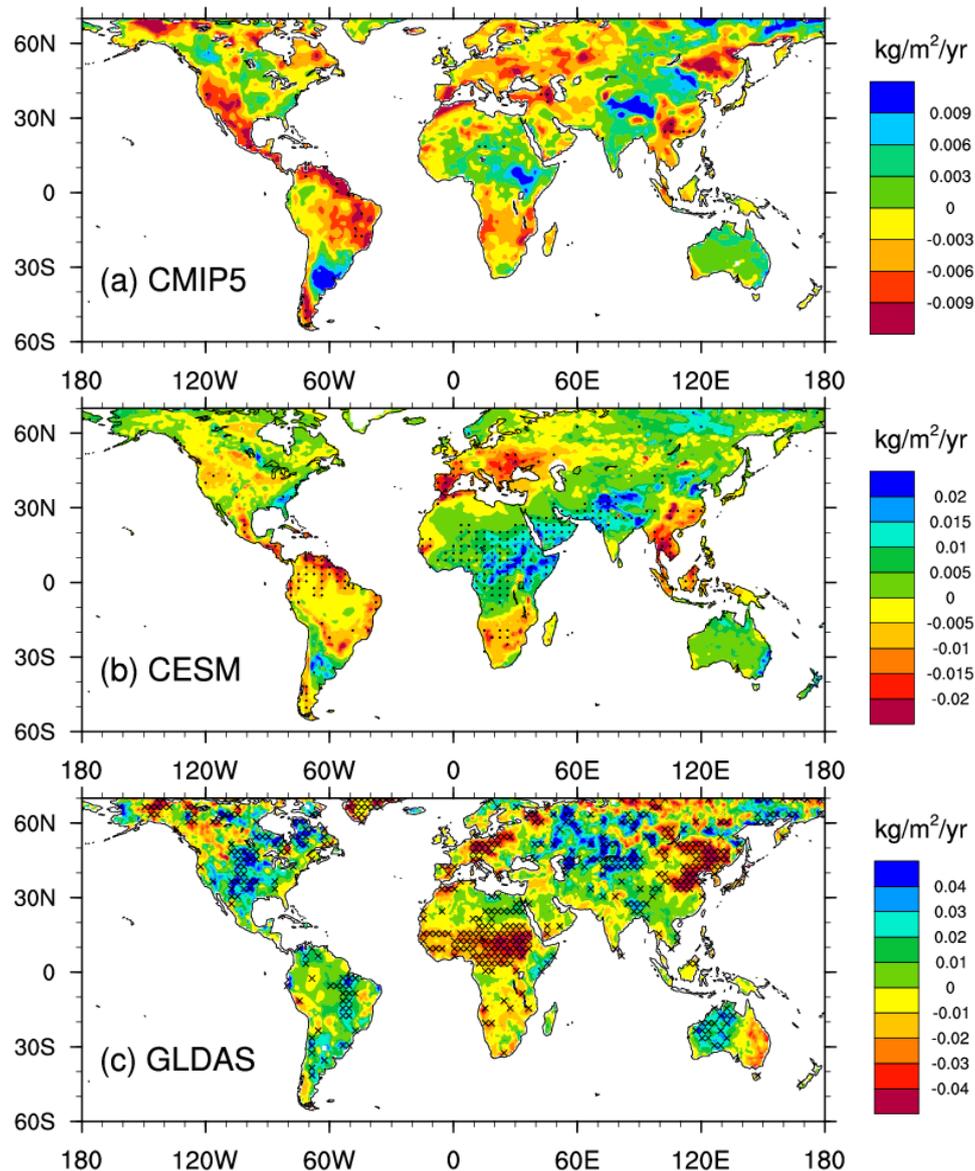
Figure 5. Spatial distributions of the annual mean SMA trend in the period 1948 – 2005 for (a) the CMIP5-EM, (b) CESM-EM, and (c) GLDAS. Dotted areas in (a) and (b) indicate more than 80% (24 of 30) of the simulations agree on the sign of change (positive or negative). The areas marked with crosses in (c) denote significant trends at the 95% confidence level according to the two-tailed Student's *t* test. Note the color scheme for each panel is different.
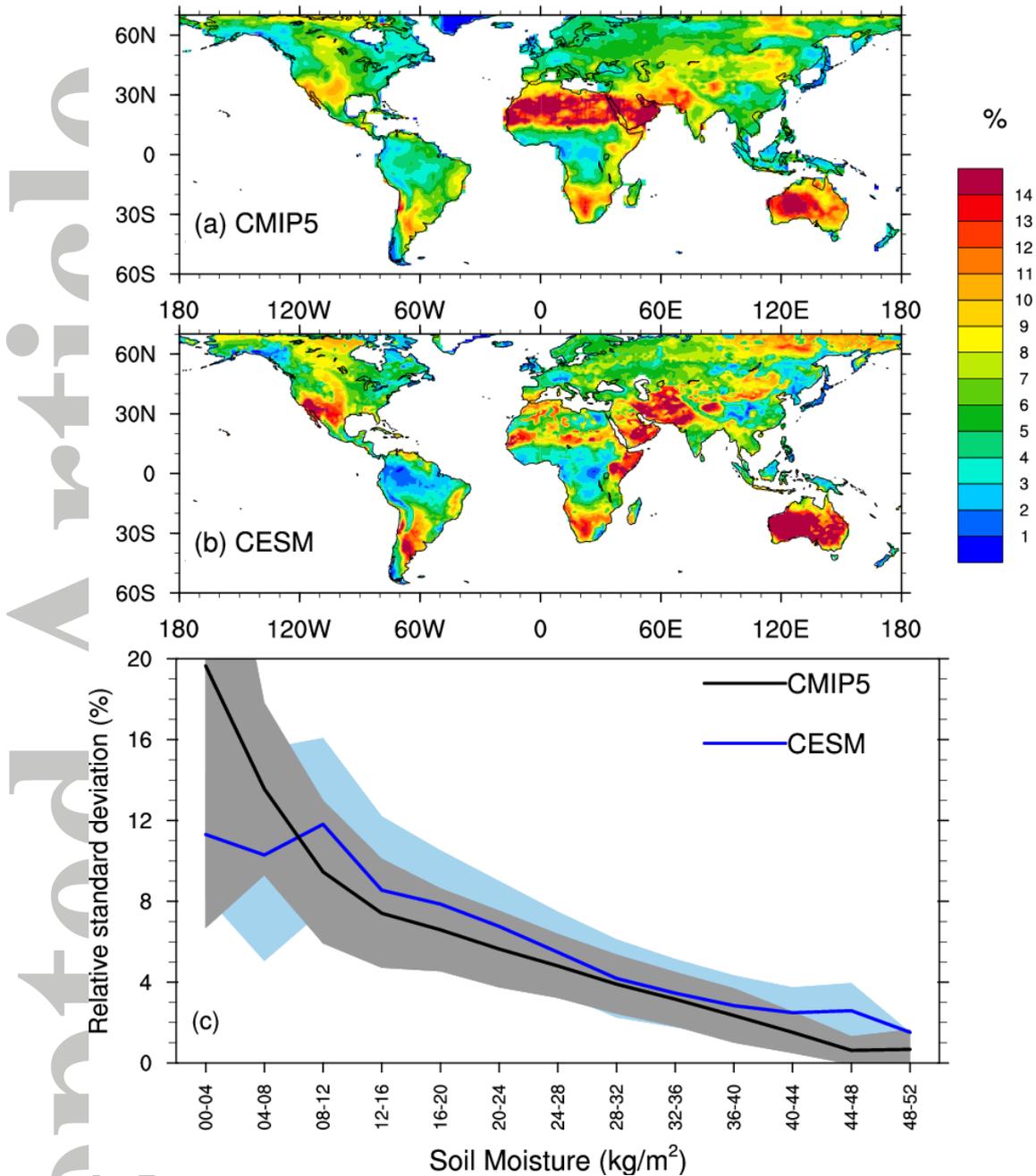
Figure 6. Spatial distributions of averaged relative standard deviation of SMA in the period 1920 – 2005 for (a) 30 CMIP5 ESMs and (b) 30 CESM simulations. (c) Relative standard deviation as a function of climatological mean soil moisture. The climatological mean soil moisture of the x-axis is the annual mean soil moisture for the period 1961 –1990. Uncertainty (shading) is one standard deviation.
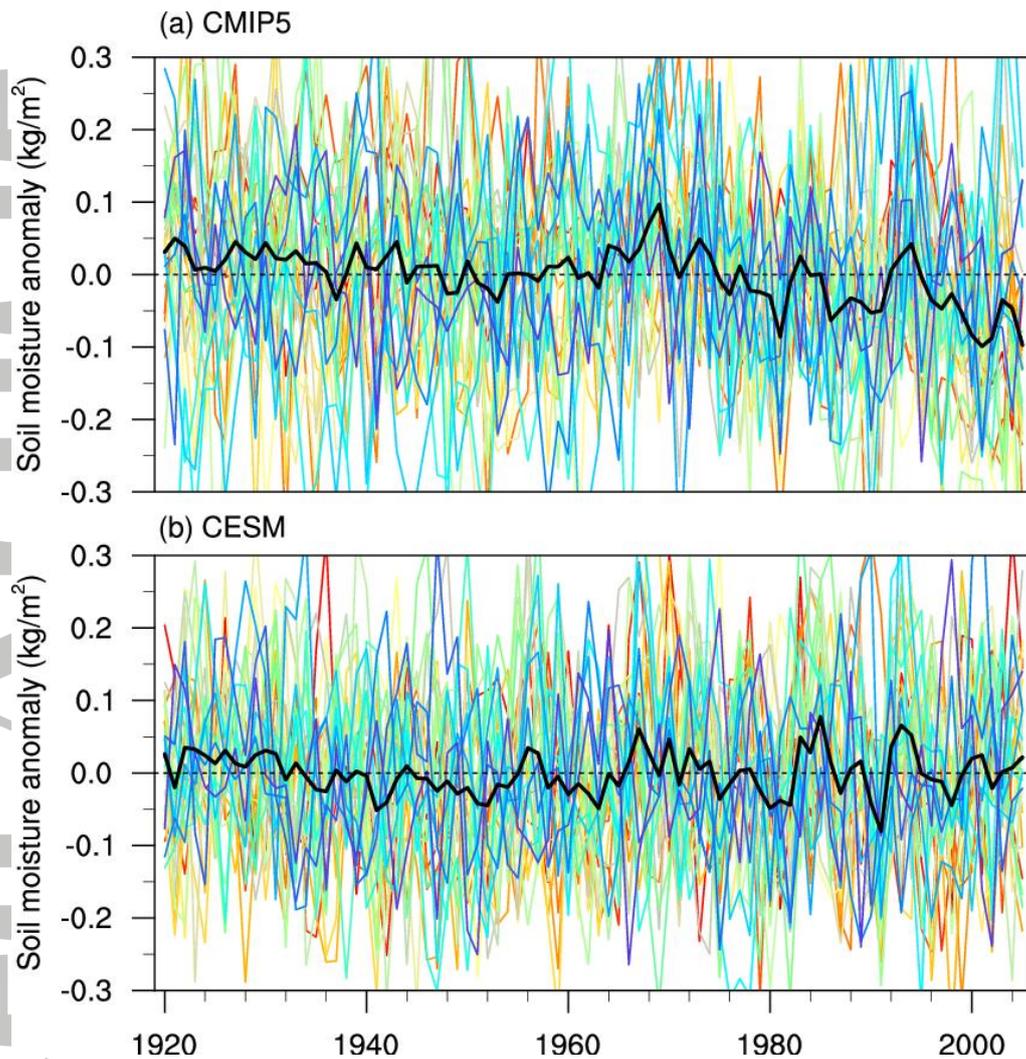
Figure 7. Time series of annual mean SMA in the period 1920 – 2005 relative to the period 1961 – 1990 for (a) 30 CMIP5 ESMs and (b) 30 CESM simulations. The colors show 30 individual members and the black curve is their ensemble mean.
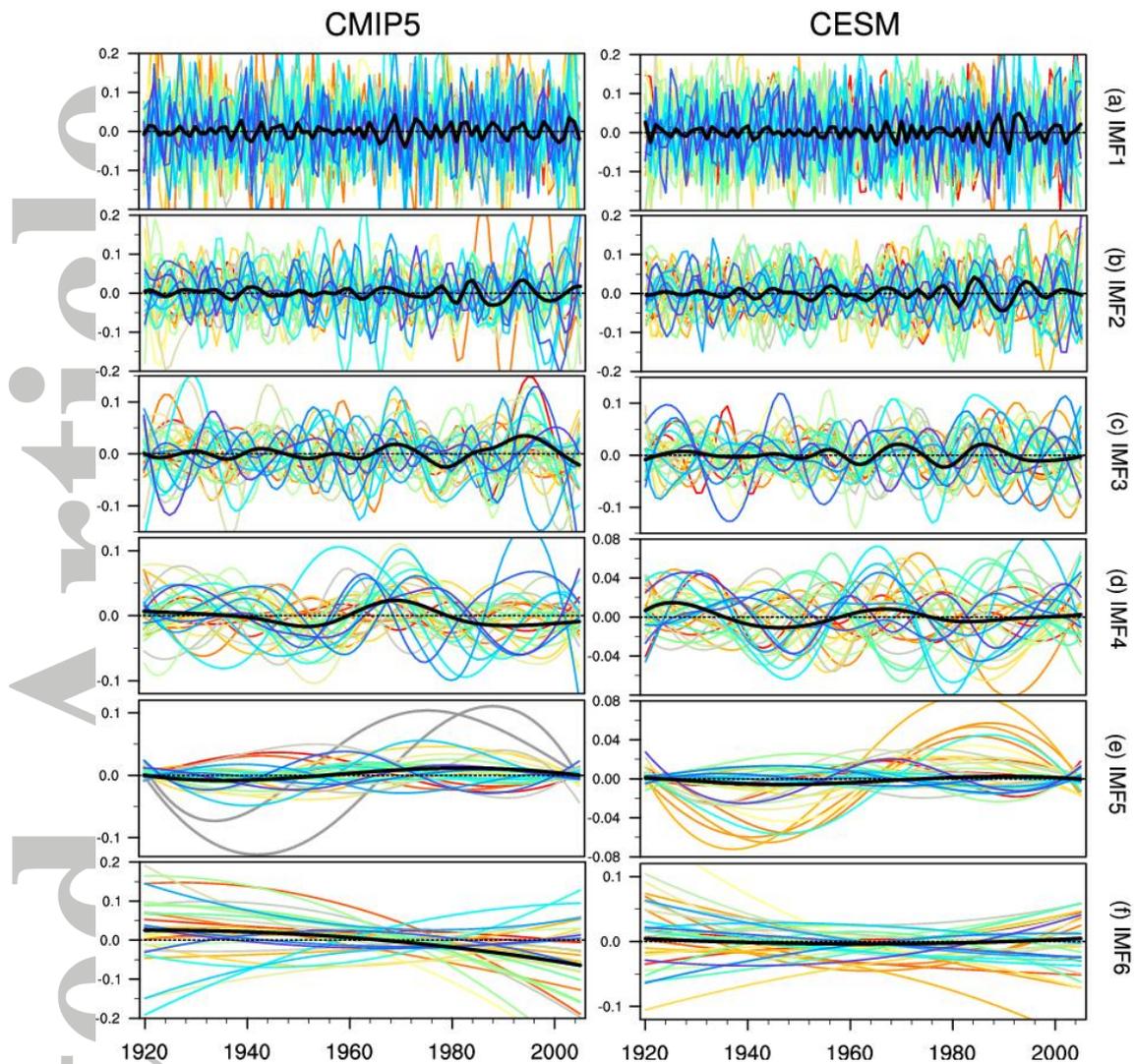
Figure 8. Time series of intrinsic mode functions (IMFs) of annual mean SMA based on ensemble empirical mode decomposition (EEMD). The colors show 30 individual members and the black curve is their ensemble mean.
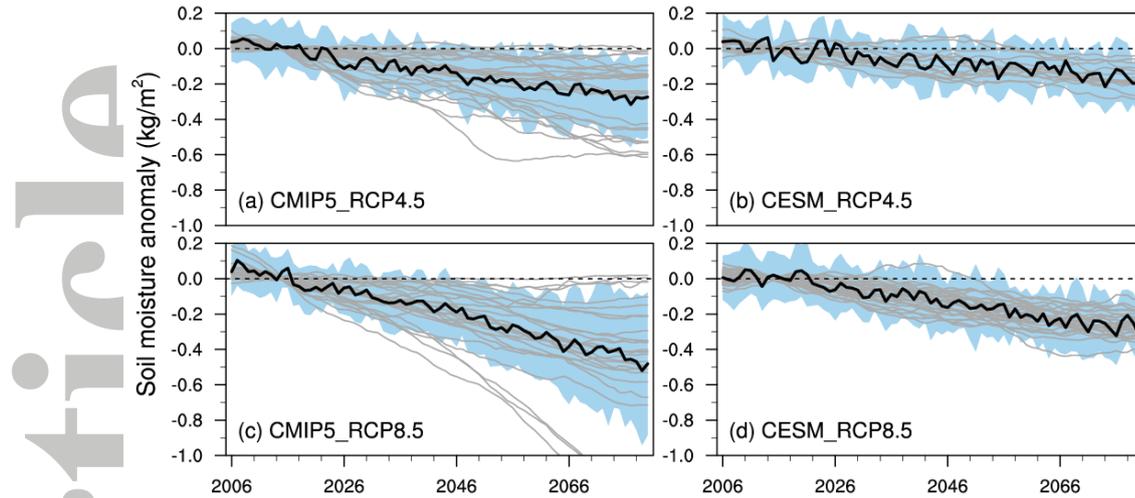
Figure 9. Same as Figure 4a, except for Representative Concentration Pathways (RCPs) in the period 2006 – 2080. The anomalies are relative to the period 2006 – 2025. The shaded area is one standard deviation. The gray curves show 20-year moving averages of 30 individual members and the black curves is their ensemble mean.
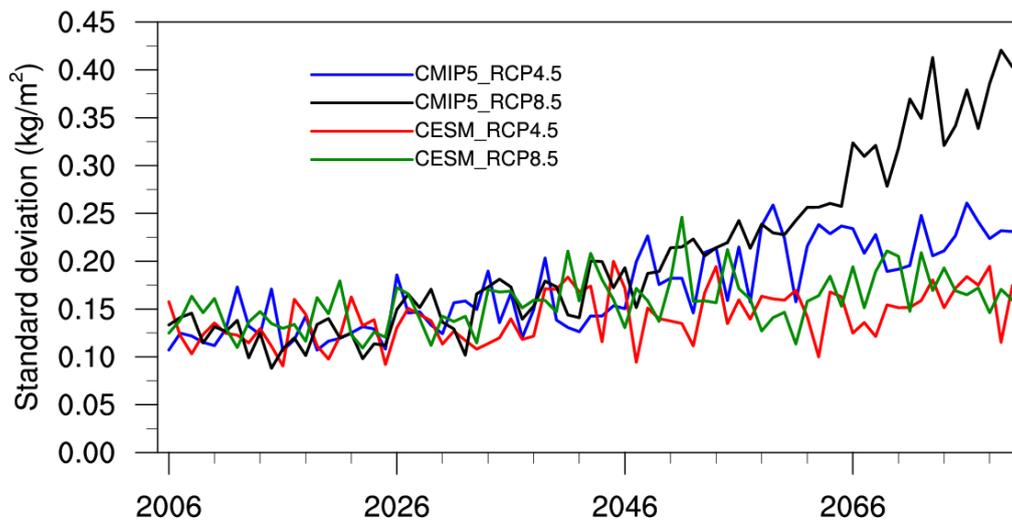
Figure 10. Time series of standard deviation of annual mean SMA for CMIP5 and CESM in the period 2006 – 2080 under RCP4.5 (blue and red) and RCP8.5 (black and green).
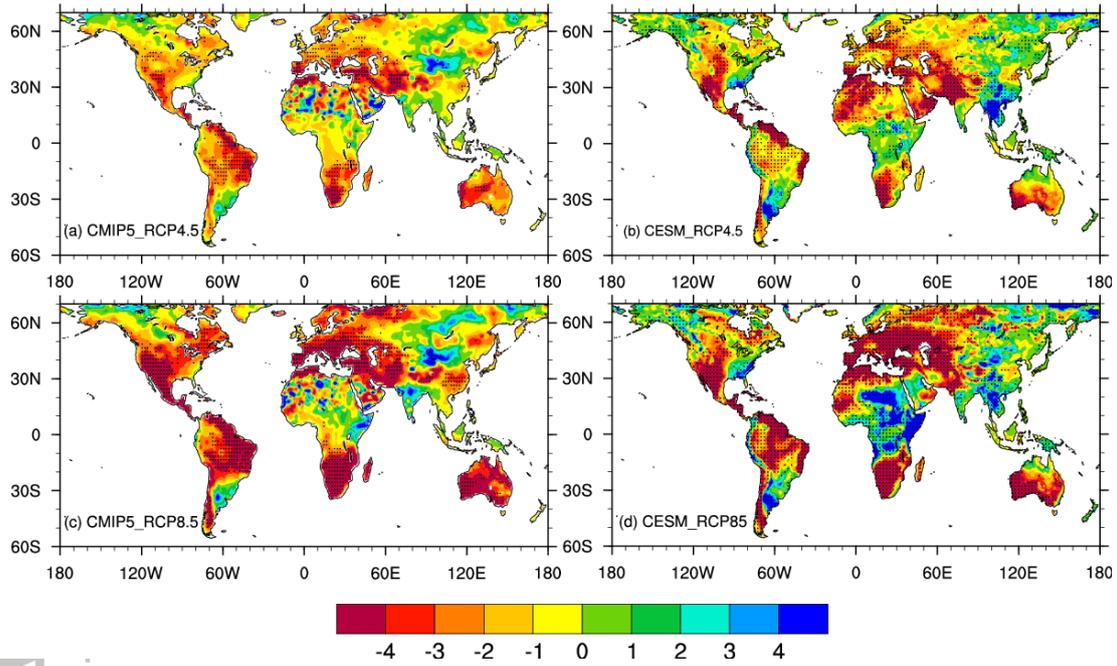
Figure 11. Percentage changes in soil moisture for the 20-year period 2061 – 2080 relative to the period 2006 – 2025. Stippling indicates that more than 80% of the models agree on the sign of change (positive or negative).